CHEMISTRY OF MATERIALS

pubs.acs.org/cm

Article

Alkali Metal Intercalation and Reduction of Layered WO_2Cl_2

Andrew I. Smith, Henry V. Wladkowski, Zachary H. Hecht, Yuqi She, Subash Kattel, Piumi I. Samarawickrama, Sarah R. Rich, Joseph R. Murphy, Jifa Tian, John F. Ackerman, William D. Rice, Elliott B. Hulley, and Brian M. Leonard*

Cite This: *Chem. Mater.* 2020, 32, 10482−10488

Read Online

ACCESS | Metrics & More | Article Recommendations | Supporting Information

ABSTRACT: Li, Na, K, Rb, and Cs have been intercalated into the two-dimensional (2D) van der Waals material WO_2Cl_2, with K, Rb, and Cs intercalation being reported for the first time. The topochemical reaction of these alkali metals causes dramatic crystallographic, optical, and electronic changes to WO_2Cl_2. During the reaction with each of the alkali metals, WO_2Cl_2 changes from a clear and transparent insulating phase to a blue partially intercalated species and finally to a lustrous bronze material. Upon intercalation, the host undergoes significant and systematic changes in interlayer spacing, as well as a 10 orders-of-magnitude change in resistivity from the base material to the intercalated bronze phase. Each of the alkali metals intercalates at a different rate and leads to specific changes in interlayer spacing and color of the bronze phase. This study provides a platform to study the electronic and optical properties of each of these new tungsten bronzes with a particular focus on lithium intercalation.

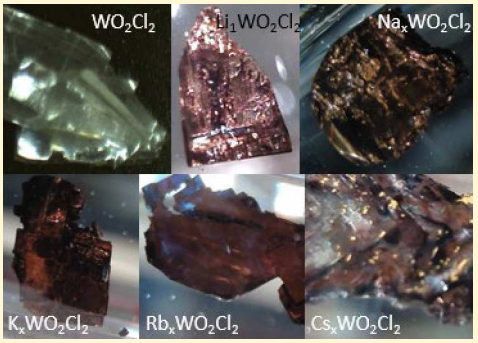

INTRODUCTION

Two-dimensional (2D) materials have been the focus of thousands of publications, ranging from smart windows to piezoelectric and ferroelectric properties and topological physics effects, for example, the quantum Hall effect.[1−4] Most of these papers focus on elemental or binary materials like graphene and transition metal dichalcogenides (TMDs).[3] With just under a thousand possible 2D materials identified, many important and novel materials have not been studied in depth.[5,6] These materials likely have a wealth of new and interesting properties that can be added to the toolbox of functional 2D materials.

One class of understudied yet exciting materials are mixed anion compounds including oxyhalides, oxynitrides, and oxychalcogenides.[7] While the oxide materials have been heavily studied because of their relation to minerology, the mixed anion analogs are relatively unexplored. These materials, with heteroleptic metal centers, offer a wealth of tunability when considering the number of anions, anion size, charge, electronegativity, and polarizability. The properties can be tuned using ideas taken from coordination chemistry like metal symmetry, coordination geometry/environment, and crystal field splitting. For example, WO_3 contains corner-sharing WO_6 octahedra with O_h symmetry around the metal atom, while WO_2Cl_2 contains corner-sharing WO_4Cl_2 octahedra with D_{4h} symmetry. The type of bonding can also be modified from covalent to ionic which can affect both the electronic structure as well as the crystal structure. WO_3 adopts a 3D crystal structure, while WO_2Cl_2 adopts a layered 2D structure. To enable more exploration of mixed anion compounds and their properties, synthetic methods need to be established, which allow for production.

This project focuses on the tungsten oxychloride, WO_2Cl_2, which has been only lightly studied and is the subject of less than 20 publications. Those investigations report the synthesis, characterization, and intercalation of WO_2Cl_2, with very little reported on its physical properties.[8−10] WO_2Cl_2 consists of corner-sharing tungsten (VI) octahedra that form tungsten−oxygen planes, which are separated by terminal chlorine atoms in the z direction, as seen in Figure 1. This arrangement results in at least two intercalation sites in the van der Waals (vdW) space, a tetrahedra hole, and a square pyramidal hole first described by Ackerman.[8] Ackerman has previously shown that that lithium can be intercalated into WO_2Cl_2 up to a 2:1 ratio, resulting in a narrow band gap n-type semiconductor.[8] P.G. Bruce then demonstrated that Na and Zn can be intercalated into WO_2Cl_2 and determined the crystallographic site where the intercalated atoms reside, with Zn occupying a tetrahedral hole (equivalent to Li[8]) and Na being four, five, six, and even eight coordinate depending on the intercalation level.[9−12] In the Na system, they found three different phases of $Na_xWO_2Cl_2$, where x = 0.25, 1, and 2. Bruce also reported

Received: August 11, 2020
Revised: November 16, 2020
Published: December 2, 2020

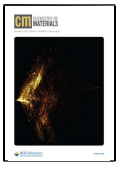

https://dx.doi.org/10.1021/acs.chemmater.0c03270
Chem. Mater. 2020, 32, 10482−10488

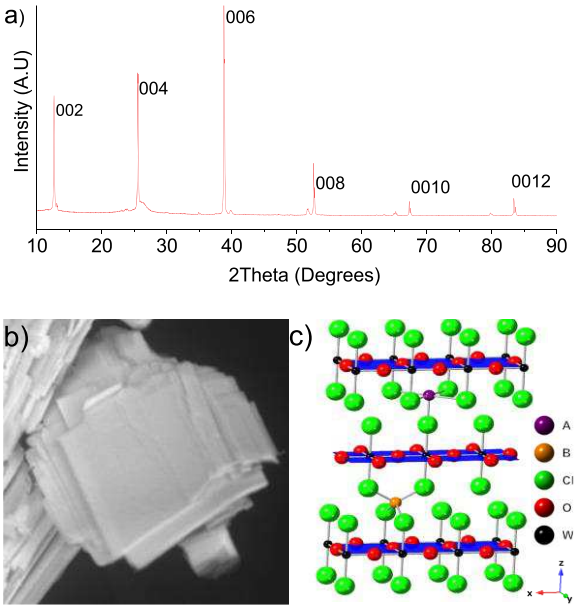

Figure 1. (a) Powder XRD of WO_2Cl_2, (b) SEM of WO_2Cl_2 (50 μm by 50 μm), and (c) crystal structure highlighting the 002 lattice planes (blue) alongside two potential intercalation sites (A and B) as determined by Ackerman (ref[7]).

the temperature dependence of Na diffusion in $Na_xWO_2Cl_2$, claiming that this system is a new member of the well-studied tungsten bronzes.[12−18]

Tungsten bronzes are a class of materials that are typically formed by reacting tungsten oxide with a second metal, often an alkali metal. They have many interesting properties, including being metallic or semiconducting, resistance to corrosion, a colorful metallic luster in their crystalline form, and exhibiting a diversity of solid phases.[13] In contrast to the tungsten bronzes, WO_2Cl_2 has a layered structure that greatly changes the intercalation chemistry as well as the materials properties. The mixed anion nature of WO_2Cl_2 provides additional tunability for the system, providing enormous potential for altering the mechanisms and kinetics of the intercalation reaction as well as the electronic, optical, and magnetic properties. In this work, we present new evidence that alkali-intercalated WO_2Cl_2 shares many, if not all, the characteristics of their three-dimensional bronze congeners.

This work focuses on the topochemical reaction of WO_2Cl_2 with three new elements, K, Rb, and Cs, giving us the complete alkali metal series to study within the same host material. The alkali metals were chosen because of their high chemical potential for reactivity, monoatomic geometries, and limited scope of investigation, including both the intercalation reactions and the properties of the resulting materials. By using an isoelectronic series of alkali intercalation species, this investigation focused on the differences in the intercalation reactions and the final products.

These reactions leave the crystals intact, which allows for both in situ and ex situ measurements on the same crystal. For example, we studied electrical resistivity of WO_2Cl_2 as a function of Li intercalation during an intercalation reaction. These experiments allowed us to probe the remarkable tunability of the WO_2Cl_2 crystal structure, including electronic and optical changes that occur upon intercalation. In addition, the alkali metal reactions allow the intercalation of metal ions with the same charge (M^+) but vastly different sizes, ranging from 0.59 Å for Li to 1.67 Å for Cs.[19] By intercalating WO_2Cl_2 with M^+ ions of increasing size, we have directly measured changes in interlayer spacing as a function of intercalant size.

RESULTS

WO_2Cl_2 was synthesized via a stoichiometric 1:2 mixture of WCl_6 and WO_3 in a Pyrex tube which was heated to 270 °C with a 20 °C gradient for 1 week. This resulted in clear, plate-like crystals up to 1 cm^2 in area. Powder X-ray diffraction (XRD), X-ray photoelectron spectroscopy (XPS), and Raman spectroscopy confirm that our synthesis results in nearly phase-pure WO_2Cl_2, as seen in Figure 1, Figure 2, and Supporting

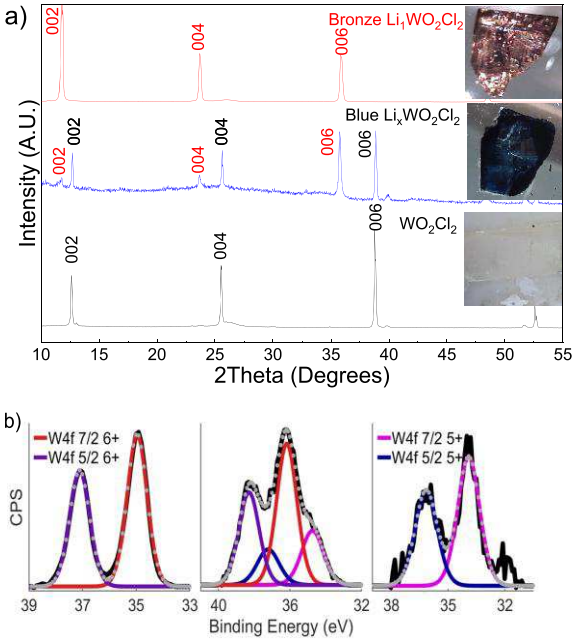

Figure 2. (a) XRD for WO_2Cl_2 (black), blue $LixWO_2Cl_2$ (blue), and bronze $Li1WO_2Cl_2$ (red), which shows that $LixWO_2Cl_2$ is composed of a mixture of the pure and bronze phases. The inset of the XRD figure shows optical images of the three phases. (b) XPS (from left to right) of WO_2Cl_2, blue $Li_xWO_2Cl_2$, and bronze $Li_1WO_2Cl_2$. The XPS region shows the W 4f peak, indicating that W in WO_2Cl_2 goes from W(VI) to a mix W^{5+} and W^{6+} in the blue phase and final bronze phase that contains only W^{5+}.

Info Figure SI1. The XRD pattern of WO_2Cl_2 agrees with literature values and is dominated by its 00l layering peaks.[20] Other minor reflections can be used to confirm the structure, but they are quite low in intensity because of the disordered stacking about the vdW layers and/or preferential orientation in the X-ray sample holder. In addition, these minor peaks are extremely difficult to monitor during the intercalation reactions; as a result, this work will primarily focus on the layering peaks of WO_2Cl_2. Scanning electron microscopy (SEM) in Figure 1(b) shows the layered, sheet-like morphology of WO_2Cl_2. Figure 1(c) shows the crystal structure of WO_2Cl_2, highlighting the 002 planes and the two intercalation sites. Site A is in the center of a square pyramid and site B is tetrahedrally coordinated to Cl's. According to previous reports, Li primarily occupies the B site, and the larger Na occupies the A site.[8,9]

Spectrum data for synthesized WO_2Cl_2 are consistent with previous studies (Figure SI1), including characteristic W=O Raman resonances at 763 and 841 cm^{-1} and terminal M-Cl

https://dx.doi.org/10.1021/acs.chemmater.0c03270
Chem. Mater. 2020, 32, 10482−10488

bonds from 400−200 cm^{-1}.[21,22] XPS studies (Figure 2(a)) confirm that tungsten is fully oxidized (W^{6+}), with measured values of 36.8 eV and 39.0 eV for $W(f_{7/2})$ and $W(f_{5/2})$ sublevels, respectively.[23]

After verifying that we could synthesize high-quality samples, large crystals of WO_2Cl_2 were intercalated with lithium in an Ar-filled glovebox using *n*-butyllithium in hexanes as a source of Li^0. While the base WO_2Cl_2 crystals appear stable in air and oxygen for extended periods of time, the alkali metal-intercalated materials undergo rapid reaction with water in air (Figure SI2) and thus were treated as air-sensitive throughout all syntheses and characterizations. During Li intercalation, WO_2Cl_2 crystals transition from clear and transparent, to blue with some transparency, and finally to a reflective opaque bronze phase [Figure 2(a) inset]. Visually similar transitions occur for all alkali metals that were intercalated into WO_2Cl_2 including Na, K, Rb, and Cs.

Lithium intercalation experiments were initially characterized by eye as being one of two phases: a blue phase or a bronze phase. The blue phase is a mixture of both the native WO_2Cl_2 and bronze phase. The bronze phase was indexed via powder diffraction data (Figure SI3) and was fit to a tetragonal unit cell (a/b = 3.76 Å and c = 15.01 Å) which has a 0.1 Å contraction in the a/b or W−O plane. The bronze phase shows a 0.57 Å expansion of the interlayer spacing, with the 002 plane of WO_2Cl_2 expanding from 6.94 to 7.51 Å [Figure 2(a)]. The lattice expansion is consistent with Shannon radii of (IV) Li^+, which corresponds with Li filling the tetrahedral site as previously reported by Ackerman.[8,19] These results are also consistent with the previously reported $Na_xWO_2Cl_2$ system where there is a bronze phase with the composition $x = 1$ and a mixture of phases at compositions $0 < x < 1$, which corresponds with our observed blue phase.[9,11]

The intercalation reaction can be quite rapid (< 10 s) at high concentrations of Li, and thus great care must also be taken to avoid partial reaction of the crystals. XRD and visual inspection of the crystals confirm that the blue phase can include an intercalated exterior and an interior with limited or no reaction and subsequent color change. XRD for these blue samples shows both the starting material WO_2Cl_2 and the intercalated phase with an expanded lattice at varying concentrations. To limit this variance in reaction completeness, lower concentrations of Li and longer reaction times were utilized to ensure that the crystals were fully intercalated. We also exfoliated the crystals with transparent tape to inspect the interior and ensure that the entire crystal was uniform by eye prior to further characterization. Phase-pure bronze crystals show no change in color throughout the crystal and have a single phase by XRD as seen in Figure 2(a).

XPS studies confirm that the transition from blue to bonze correlates with the extent of W reduction. XPS of the bronze phase shows only W^{+5} and the blue phase shows partial reduction of the host, with W^{+6} and W^{+5} being present (Figure 2(b)). If each W^{+5} atom corresponds to one Li atom intercalated, the data are consistent with a chemical formula of $Li_xWO_2Cl_2$, with $x < 1$ for the blue phase and $Li_1WO_2Cl_2$ for the bronze phase. XPS and XRD results complement each other, with the bronze sample being a single phase via XRD, showing only W^{+5} via XPS, and the blue phase being mixed via both XRD and XPS.

Electrical experiments show that electrical conductivity is dependent upon the extent of Li intercalation. Resistances were monitored using two leads which were attached to a large crystal of WO_2Cl_2 with silver epoxy. The crystal was reacted with a 0.25 M solution of *n*-butyllithium in hexanes, while simultaneously measuring the resistance and taking images to observe the color changes (Figure 3). Initially, an insulator

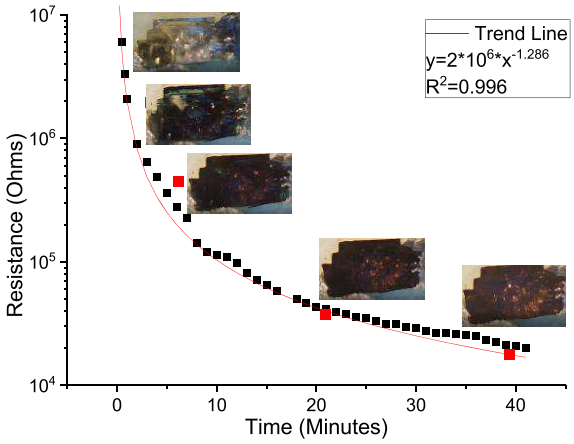

Figure 3. Two-point resistivity data and optical images of a crystal of WO_2Cl_2 during intercalation with Li via 0.25 M *n*-butyllithium in hexanes. The optical images of the crystal were taken at the start of the reaction and then at 1, 4, 20, and 40 min as noted by the red squares.

with a resistance >100 MΩ, within a few minutes WO_2Cl_2 quickly turns blue, and as the reaction progresses, regions of the crystals become bronze in color. In this experiment, it required a full 20 minutes for the WO_2Cl_2 to become completely bronze in color. Although bronze in exterior color, intercalation continued to happen, as the interior of the crystal is the last to be fully intercalated. This sample reached a final resistance of 685 Ω (Figure SI4), giving a range of at least 4 orders of magnitude. Two-point temperature-dependent resistance measurements on separate crystals of the blue $Li_xWO_2Cl_2$ phase show that it exhibits semiconducting behavior (Figure SI5). While the temperature-dependent measurements on the bronze $Li_1WO_2Cl_2$ also showed semiconducting-like behavior, these measurements were complicated by the reactivity of the bronze crystals with the Ag conducting epoxy (Figure SI6). The edges of the crystals noticeably changed at the points of attachment, and it is possible that ammines, phenols, and other compounds that make up the epoxy may have reacted with the surface of the crystal, producing non-Ohmic contact points. The change in resistivity of crystals during lithium intercalation was monitored for a series of individual crystals with known dimensions, revealing resistivity changes from >100 MΩ·cm (WO_2Cl_2) to 0.01 Ω·cm ($Li_1WO_2Cl_2$), a change of at least 10 orders of magnitude (Figure SI7). Additional four-point measurements at room temperature confirmed the dramatic change in resistivity (Figure SI8). These data and data from other experiments have been fit to a simple exponential reminiscent of Fick's laws of diffusion (Figure 3), suggesting that the intercalation reaction is diffusion-limited.

To better understand the optical transitions observed during intercalation, absorption measurements were carried out both in the transmission geometry and using an integrating sphere. Absorption spectra (Figure 4) exhibit a marked increase in the overall absorption between WO_2Cl_2 and $Li_xWO_2Cl_2$, where an absorption feature peak at 1240 nm, leads to the characteristic blue color of $Li_xWO_2Cl_2$. The absorption in the red and near

https://dx.doi.org/10.1021/acs.chemmater.0c03270
Chem. Mater. 2020, 32, 10482−10488

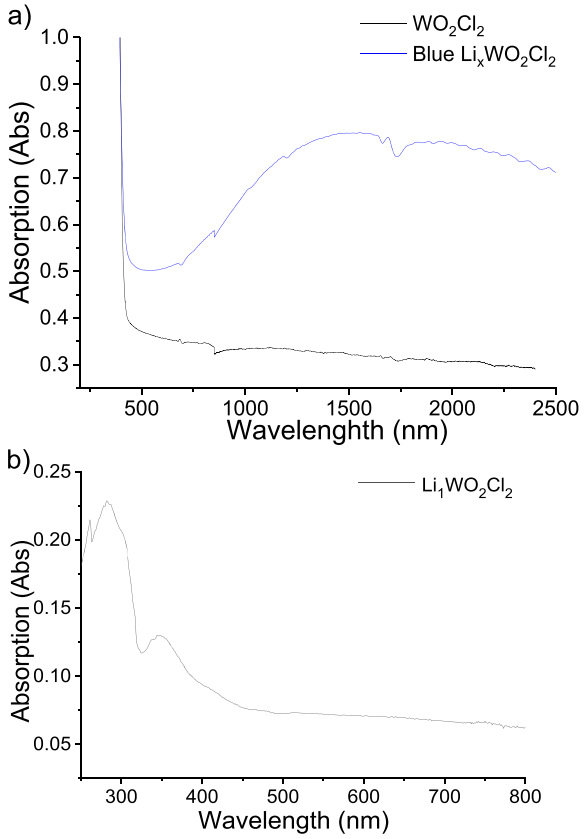

Figure 4. (a) Absorption spectra taken of WO_2Cl_2 and $Li_xWO_2Cl_2$ (blue) in transmission mode, showing a remarkable increase in absorption between the base material and the blue phase. (b) $Li_1WO_2Cl_2$ (bronze) absorption spectra measured with an integrating sphere due to its opacity. The bronze phase is largely reflective in the visible region with some absorption in the UV.

IR is characteristic of a d-d transition and further evidence of Li donating its electron to the host. Bronze $Li_1WO_2Cl_2$ shows remarkably little absorption in the visible region using an integrating sphere, giving indirect evidence of strong reflection that is characteristic of the related tungsten bronze materials.[24]

To estimate the increase in conductivity created by the alkali intercalation, we used terahertz (THz) time-domain spectroscopy (TTDS) to measure various levels of Li-intercalated WO_2Cl_2 without contact. Because of the extreme air and water vapor sensitivity, we were not able to polish these crystals, so scattering was a significant effect. However, the change in the conductivity between WO_2Cl_2 and Li-intercalated WO_2Cl_2 is, to first order, a measure of the change in the conductivity from an increase in the carrier concentration obtained from Li intercalation.

TTDS measurements were taken between 0.2 and 2.7 THz through a cryostat at room temperature with z-cut quartz windows using a ∼ 200 uJ/pulse, Ti:S amplifier laser with a 1 kHz repetition rate. To prevent degradation, we mounted the WO_2Cl_2 crystals in an Ar-filled cryostat inside of an Ar-purged glovebox. We used optical rectification with a ZnTe crystal to generate linearly polarized THz pulses, which were then collimated and focused onto the WO_2Cl_2 crystals using gold-coated parabolic mirrors. The digitally boxcar-averaged THz electric field was measured using electro-optical sampling with a co-propagating 800 nm, ∼200 fs pulses on a < 110> cut, 1 mm thick ZnTe crystal, and a balanced detector. Transmitted electric fields were referenced to a well-defined aperture in the cryostat.

To avoid any changes in the conductivity due to crystal degradation, we performed a single THz scan immediately after the glovebox transfer of the sample into the cryostat. Figure 5(a) shows time-domain THz electric field traces for

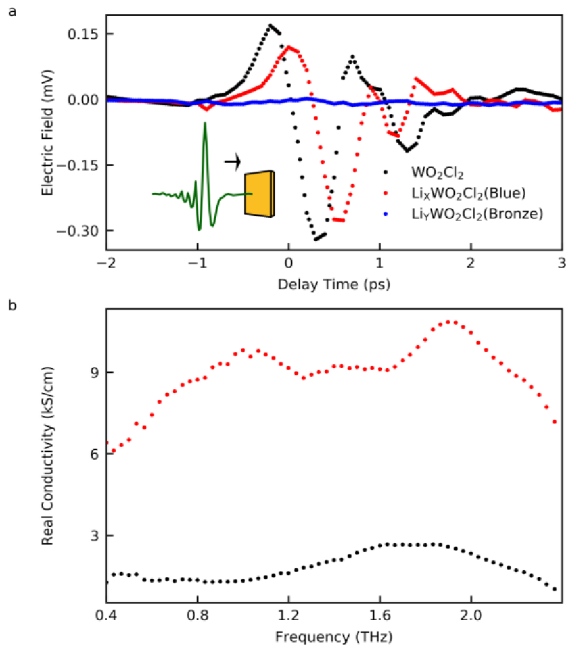

Figure 5. Terahertz (THz) spectroscopy measurements of WO_2Cl_2 crystals with different Li intercalation concentrations. (a) Time domain THz traces illustrating the decrease in THz transmission as the intercalation concentration increases. (b) Real conductivity for each unpolished WO_2Cl_2 crystal calculated from the THz transmission spectra. As Li intercalation concentration increases, the real conductivity increases. Because of the lack of THz transmission with the bronze Li-intercalated WO_2Cl_2 crystal, reliable conductivity estimates could not be made.

each of the three WO_2Cl_2 crystals that we examined. As the Li intercalation concentration increases, a parameter controlled by the duration the WO_2Cl_2 spent immersed in *n*-butyllithium, the THz electric field decreases. In fact, despite being similar in thickness to the other WO_2Cl_2 crystals, the most intercalated crystal (bronze $LiWO_2Cl_2$) admits barely any transmitted THz.

To estimate the crystal optical conductivity spectral behaviors, we converted the time-domain THz measurements to the frequency domain using a fast Fourier transform and then computed the real and imaginary conductivities. As seen in Figure 5(b), the real conductivity for the unintercalated WO_2Cl_2 increases by roughly a factor of four upon partial intercalation. As stated above, the relative ratio of the conductivity is the most meaningful physical quantity here because we are performing a transmission measurement on unpolished crystals. Because of the lack of THz transmission (which we are attributing to the high degree of intercalation), we could not reliably obtain precise conductivity data for the fully intercalated crystal.

Given that the integral of the real conductivity across all relevant frequencies is directly related to the carrier concentration (and inversely proportional to the effective mass), the relative increase in conductivity of the partially Li-intercalated WO_2Cl_2 to the WO_2Cl_2, which is roughly a factor

https://dx.doi.org/10.1021/acs.chemmater.0c03270
Chem. Mater. 2020, 32, 10482−10488

of six, strongly suggests that the intercalating Li atoms donate an electron to the host WO_2Cl_2 crystal lattice. The increased electron concentration is assumed to be responsible for the observed relative increase in the WO_2Cl_2 conductivity. Measurements over a larger bandwidth and with polished crystals would allow for a quantitative and accurate measure of both the true conductivity and carrier concentration of the intercalated WO_2Cl_2 crystals.

XRD and Raman spectroscopy on blue $Li_xWO_2Cl_2$ further support that the mechanism of lithium intercalation happens layer by layer. The blue phase (Figure 2) clearly shows the base material (6.94 Å) and the bronze phase (7.51 Å), which suggests that intercalation happens layer by layer starting with a few individual layers which accept the electrons and their adjacent vdW layers accepting the Li ions. When these layers reach a 1:1 W:e^- ratio, additional layers begin the reaction. Raman spectra collected from various samples of $Li_xWO_2Cl_2$ show that Li intercalation does not shift peak positions (Figure SI1). The only apparent change in the Raman signature of $Li_xWO_2Cl_2$ was the dramatic loss of peak intensity. This seemed to loosely correlate with intercalation, with the bronze phase being highly conductive and reflective in nature which limits how far the Raman probe beam could sample the crystal. The lack of observable change in Raman mode frequency as a function of Li intercalation gives strong evidence that a few Li^+ ions and their donated electrons are locally bound to a few layers and produce layers that are highly conductive and reflective in nature, with unreacted layers being solely responsible for the Raman signal.

Na, K, Rb, and Cs have also been successfully intercalated into WO_2Cl_2 using *n*-butylsodium, benzylpotassium, benzlyrubidium, and benzylcesium, respectively. These reactions were also monitored by color change with the same blue to bronze transitions observed in each system. The time it took for the bronze phase to appear varied greatly; Na became bronze after a few days and Cs required months. Li and Na produced bronze crystals very similar in color to each other, with the larger alkali metals producing bronze crystals with a more reddish hue (Figure SI9). Based on these observed color changes, we hypothesized that each of the alkali metals produces the same insulator to bronze transition that is found in the Li system and previously reported for Na reactions.[12]

XRD of the alkali metal samples shows the successful intercalation of Na, K, Rb, and Cs into WO_2Cl_2, with interlayer spacing increasing with the atom size (Figure 6). These expansions were then compared to the Shannon radii of each element with different coordination numbers [Figure 6(b) and inset table[19]]. Using a simple linear fit model, we conclude that Na and K are six coordinate and Rb and Cs were eight coordinate. The resulting graph from Li, Na, K, and Rb is in very good agreement with the Shannon radii, suggesting that these alkali metals intercalated into WO_2Cl_2. Cs shows the lowest levels of intercalation (via XRD); this is likely due to its very large size. Additionally, its expansion of 1.96 Å is 23% larger than the observed trend for the Li−Rb model. This suggests that Cs may be causing layer rearrangement and may be intercalated into an as yet unknown site. Future experiments are needed to confirm our model and to understand the Cs intercalated phase.

Energy-dispersive X-ray spectroscopy (EDS), transmission electron microscopy (TEM), and SEM further confirm that Na, K, Rb, and Cs intercalation is uniform throughout the entire crystal (Figure 7 shows that EDS is not possible for Li)

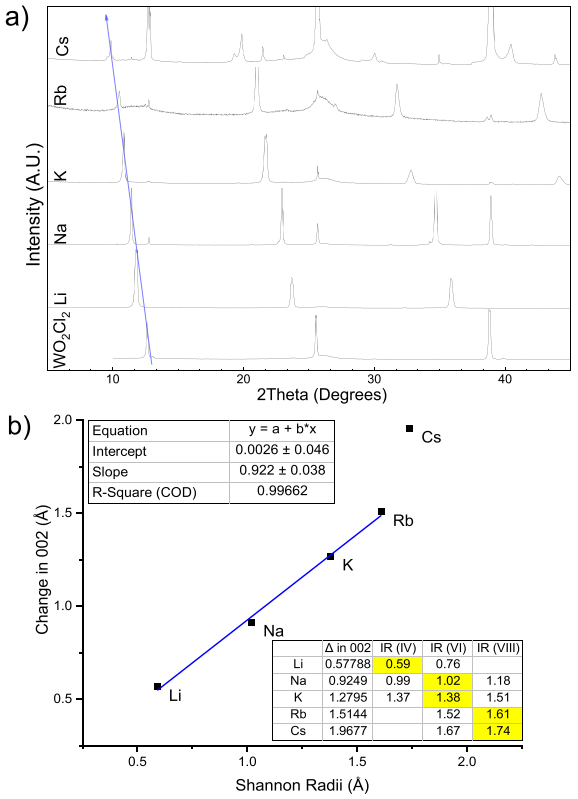

Figure 6. (a) XRD of WO_2Cl_2 that has been intercalated with Li, Na, K, Rb, and Cs. Change in 00l (interlayer spacing) can clearly be seen as the intercalated ion size increases. (b) Plot of the change in interlayer spacing (00l) vs the known Shannon radii. The inset table shows different ionic radii (IR) of each ion with multiple coordination numbers.

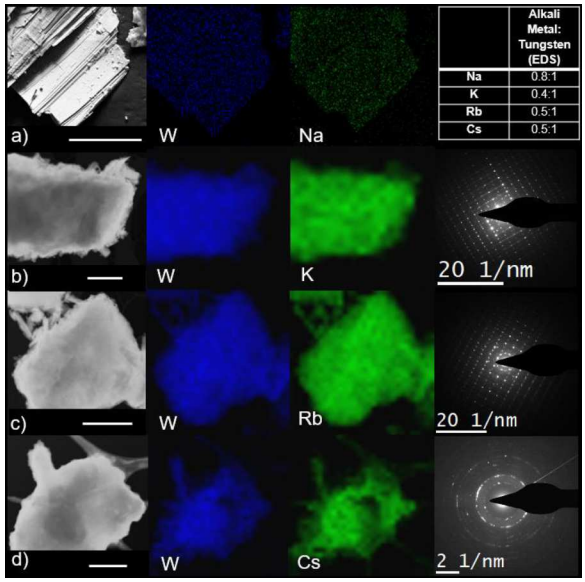

Figure 7. (a) SEM and the corresponding EDS maps showing uniform Na intercalation in WO_2Cl_2 (scale bar 200 μm), (b−d) TEM and the corresponding EDS maps showing uniform K, Rb, and Cs intercalation into WO_2Cl_2 (all scale bars 500 nm) and SAED for each sample. A table shows the ratio of alkali metal to tungsten from EDS.

with up to 0.8 Na atoms per W, 0.4 K per W, and a 0.5 per W ratio for Rb and Cs. These data suggest that the reaction did not proceed with the same concentration as Li samples. Both

https://dx.doi.org/10.1021/acs.chemmater.0c03270
Chem. Mater. 2020, 32, 10482−10488

TEM and SEM show that morphology of the crystals does not change during intercalation, with all samples consistently exhibiting plate-like morphology (Figure 7). Additionally, the crystallinity of the system is largely preserved during intercalation as revealed by sharp peaks in the XRD (Figure 6) and the well-defined points in the selected area electron diffraction (SAED) (Figure 7). Lattice fringes were observed in every sample, which confirmed the crystallinity, as seen in Figure SI12. XPS detailed in Figures SI16−19 shows the presence of Na, K, Rb, and Cs alongside W^{+6} and W^{+5}. Given the surface-sensitive nature of XPS, we were not surprised to see an excess of K and Rb on the surface of our crystals. This is likely from excess K and Rb reagents decomposing onto the surface of crystals in the form of salts. Using the EDS values for a baseline, this study shows so far that most alkali metals cannot be intercalated into WO_2Cl_2 to a 1:1 ratio; however, we believe that the observed alkali concentrations are limited by our experimental method. We plan to study the limits of alkali metal intercalation in future studies.

CONCLUSIONS

In this work, we have investigated the 2D van der Waals material WO_2Cl_2, highlighting its remarkable ability to tune the crystallographic, electronic, and optical properties via topochemical reaction with alkali metals. We have evidence of an insulator to bronze transition for WO_2Cl_2, with $Li_1WO_2Cl_2$ significantly reducing THz radiation, reflecting visible light, and having a 10 orders-of-magnitude change in resistivity. In addition to lithium, Na, K, Rb, and Cs were also intercalated into WO_2Cl_2, which showed a dramatic change in the reaction rate as the ion size increased, even though they are isoelectronic. The change in interlayer spacing for Li, Na, K, and Rb shows incredible agreement with Shannon's radii, offering some insight into the coordination environment within the vdW region. It is anticipated that the electrical and optical properties of the other alkali metals are likely very similar to the Li analog; however, a shift in the color of the bronze phase was observed, which is worthy of continued investigation. This work successfully demonstrates the synthesis of both WO_2Cl_2 and a new series of 2D tungsten bronzes via intercalation of the alkali metals and sets the stage for further investigation into the interplay between the structural changes that alkali metal intercalation can have on van der Waals materials and how it may affect their optical and electronic properties.

EXPERIMENTAL SECTION

All reagents are from Sigma-Aldrich and were used as received. WO_2Cl_2 was directly synthesized from a 2:1 ratio of WO_3 and WCl_6 in an evacuated Pyrex tube with a thermal gradient of 270 to 250 °C for 7 days. The intercalation reactions were all done within an Ar-filled glovebox with water and oxygen levels below 0.1 ppm. Lithium intercalation was carried out in 20 mL of hexanes with 2.5 M *n*-butyllithium in hexanes. Sodium, potassium, rubidium, and cesium intercalations were carried out in 20 mL of toluene with *n*-butylsodium, benzylpotassium, benzlyrubidium, and benzylcesium. Each of the alkali metals was prepared according to previous works.[25−27] The time scale for these intercalation reactions varied from minutes for Li, weeks for Na and K, to several months for Rb and Cs.

Phase purity was confirmed by XRD using a Rigaku Smart Lab X-ray diffractometer; samples were sealed with Mylar and vacuum grease to maintain an oxygen- and moisture-free environment. Raman scattering of the WO_2Cl_2 crystal was carried out using a custom-built sample chamber attached to a five-axis translational and tilt platform. The sample chamber was flooded with Ar gas to avoid crystal degradation during measurements. A plasma-line-filtered 632.8 nm laser (1.54 mW) was propagated through a long-working distance Mitutoyo 50x (NA = 0.42) objective (spot size = 1 μm). The scattered light, which was collected via the same objective lens, was resolved using a 1200 L/mm grating, Isoplace 320 mm spectrometer, and a liquid nitrogen-cooled charge-coupled device. Absorption data collected through transmission mode were collected by a Jasco V-670 spectrophotometer, with samples thinned via tape and then mounted with vacuum grease onto an Al sample holder. $Li_1WO_2Cl_2$ absorption data were collected with a PerkinElmer Lambda 950 UV/VIS Spectrometer with a 150 mm InGaAs integrating sphere module. Terahertz (THz) time-domain spectroscopy measurements were taken between 0.2 and 2.7 THz through an Ar-purged cryostat with z-cut quartz windows using a ∼200 uJ/pulse and a 1 kHz repetition rate Ti:S amplifier laser. To prevent degradation, we mounted the WO_2Cl_2 crystals in an Ar-filled cryostat inside of an Ar-purged glovebox. We used optical rectification in a ZnTe crystal to generate linearly polarized THz pulses, which were then collimated and focused onto the WO_2Cl_2 crystals using gold-coated parabolic mirrors. The digitally boxcar-averaged THz electric field was measured using electro-optical sampling with a co-propagating 800 nm, ∼200 fs pulses on a < 110> cut, 1 mm thick ZnTe crystal, and a balanced detector. Transmitted electric fields were referenced to a well-defined aperture in the cryostat. Time-dependent resistivity measurements were collected with a Keithly 2401 Source Meter, and optical images were collected with a USB microscope. TEM images were collected on samples that had been ground with a mortar and pestle, suspended in toluene, and then drop-cast onto lacey Cu grids with a FEI Tecnai G2 F20 200 kV (S) transmission electron microscope. XPS was carried out using a Kratos Ultra DLD X-ray Photoemission Spectrometer. SEM images were collected with a FEI QUANTA 450 with a Shottky Field Emitter Gun.

ASSOCIATED CONTENT

Supporting Information

The Supporting Information is available free of charge at https://pubs.acs.org/doi/10.1021/acs.chemmater.0c03270.

Raman spectroscopy, electrical measurements, optical images, XRD, SEM and EDS mapping, and XPS data (PDF)

AUTHOR INFORMATION

Corresponding Author

Brian M. Leonard − *University of Wyoming, Laramie, Wyoming 82072, United States;* orcid.org/0000-0002-9185-2473; Email: bleonar5@uwyo.edu

Authors

Andrew I. Smith − *University of Wyoming, Laramie, Wyoming 82072, United States*

Henry V. Wladkowski − *University of Wyoming, Laramie, Wyoming 82072, United States*

Zachary H. Hecht − *University of Wyoming, Laramie, Wyoming 82072, United States*

Yuqi She − *University of Wyoming, Laramie, Wyoming 82072, United States*

Subash Kattel − *University of Wyoming, Laramie, Wyoming 82072, United States*

Piumi I. Samarawickrama − *University of Wyoming, Laramie, Wyoming 82072, United States*

Sarah R. Rich − *University of Wyoming, Laramie, Wyoming 82072, United States*

Joseph R. Murphy − *University of Wyoming, Laramie, Wyoming 82072, United States*

https://dx.doi.org/10.1021/acs.chemmater.0c03270
Chem. Mater. 2020, 32, 10482−10488

Jifa Tian − *University of Wyoming, Laramie, Wyoming 82072, United States;* orcid.org/0000-0003-2921-470X
John F. Ackerman − *University of Wyoming, Laramie, Wyoming 82072, United States*
William D. Rice − *University of Wyoming, Laramie, Wyoming 82072, United States*
Elliott B. Hulley − *University of Wyoming, Laramie, Wyoming 82072, United States;* orcid.org/0000-0002-2630-3689

Complete contact information is available at: https://pubs.acs.org/10.1021/acs.chemmater.0c03270

Author Contributions

The manuscript was written through contributions of all authors. All authors have given approval to the final version of the manuscript.

Notes

The authors declare no competing financial interest.

■ ACKNOWLEDGMENTS

This work was supported by NSF-DMR 1905914. S.R.R. and B.M.L. were also supported by NSF-CHE-1358498.

■ REFERENCES

(1) Geim, A. K.; Novoselov, K. S. The Rise of Graphene. *Nat. Mater.* **2007**, *6*, 183−191.
(2) Mounet, N.; Gibertini, M.; Schwaller, P.; Campi, D.; Merkys, A.; Marrazzo, A.; Sohier, T.; Castelli, I. E.; Cepellotti, A.; Pizzi, G.; Marzari, N. Two-Dimensional Materials from High-Throughput Computational Exfoliation of Experimentally Known Compounds. *Nat. Nanotechnol.* **2018**, *13*, 246−252.
(3) Krishnan, U.; Kaur, M.; Singh, K.; Kumar, M.; Kumar, A. A Synoptic Review of MoS 2 : Synthesis to Applications. *Superlattices Microstruct.* **2019**, *128*, 274−297.
(4) Li, X.; Tao, L.; Chen, Z.; Fang, H.; Li, X.; Wang, X.; Xu, J. B.; Zhu, H. Graphene and Related Two-Dimensional Materials: Structure-Property Relationships for Electronics and Optoelectronics. *Appl. Phys. Rev.* **2017**, *4*, No. 021306.
(5) Geim, A. K.; Grigorieva, I. V. Van Der Waals Heterostructures. *Nature* **2013**, *499*, 419−425.
(6) Ashton, M.; Paul, J.; Sinnott, S. B.; Hennig, R. G. Topology-Scaling Identification of Layered Solids and Stable Exfoliated 2D Materials. *Phys. Rev. Lett.* **2017**, *118*, 106101.
(7) Kageyama, H.; Hayashi, K.; Maeda, K.; Attfield, J. P.; Hiroi, Z.; Rondinelli, J. M.; Poeppelmeier, K. R. Expanding Frontiers in Materials Chemistry and Physics with Multiple Anions. *Nat. Commun.* **2018**, *9*, 1−15.
(8) Ackerman, J. F. Lithium Intercalation of WO2Cl2. *Mater. Res. Bull.* **1988**, *23*, 165−169.
(9) Bruce, P. G.; Nowinski, J.; Gibson, V. C.; Hauptman, Z. V.; Shaw, A. Sodium Intercalation into WO2Cl2. *J. Solid State Chem.* **1990**, *89*, 202−207.
(10) Bruce, P. G.; Krok, F.; Lightfoot, P.; Nowinski, J. L.; Gibson, V. C. Multivalent Cation Intercalation. *Solid State Ionics* **1992**, *53-56*, 351−355.
(11) Abrahams, I.; Nowinski, J. L.; Bruce, P. G.; Gibson, V. C. Structure of the Intercalate NaWO2Cl2. *J. Solid State Chem.* **1991**, *94*, 254−259.
(12) Bruce, P. G.; Nowiński, J.; Gibson, V. C. Temperature Dependence of Sodium Ion Diffusion in Nax WO2Cl2. *Solid State Ionics* **1992**, *50*, 41−45.
(13) Dickens, P. G.; Whittingham, M. S. The Tungsten Bronzes and Related Compounds. *Q. Rev., Chem. Soc.* **1968**, *22*, 30−44.
(14) Magnéli, A.; Virtanen, A. I.; Olsen, J.; Virtanen, A. I.; Sörensen, N. A. Studies on the Hexagonal Tungsten Bronzes of Potassium, Rubidium, and Cesium. *Acta Chem. Scand.* **1953**, *7*, 315−324.
(15) Tegg, L.; Cuskelly, D.; Keast, V. J. Plasmon Responses in the Sodium Tungsten Bronzes. *Plasmonics* **2018**, *13*, 437−444.
(16) Straumanis, M. E.; Dravnieks, A. The Sodium Tungsten Bronzes. II. The Electrical Conductivity of the Bronzes. *J. Am. Chem. Soc.* **1949**, *71*, 683−687.
(17) Dickens, P. G.; Quilliam, R. M. P.; Whittingham, M. S. The Reflectance Spectra of the Tungsten Bronzes. *Mater. Res. Bull.* **1968**, *3*, 941−949.
(18) Brown, W.; B, B.; Banks, E.; Brimm, E. O.; Brantley, J. C.; Lorenz, J. H.; Jellinek, H. The Sodium Tungsten Bronzes. *J. Am. Chem. Soc* **1954**, *76*, 963−966.
(19) Shannon, R. D.; Revised Effective Ionic Radii and Systematic Studies of Interatomie Distances in Halides and Chaleogenides. *Central Research and Development Department, Experimental Station, E. L Du Pont de Nemours The Effective Ionic Radii of Shannon and Prewitt.* 1976.
(20) Abrahams, I.; Nowinski, J. L.; Abrahams, I.; Gibson, V. C. The Disordered Structure of Wo2cl2: A Powder Diffraction Study. *J. Solid State Chem.* **1993**, *102*, 140−145.
(21) Adams, D. M.; Churchill, R. G. The Vibrational Spectra of Some Oxide Halides of Molybdenum and Tungsten. *J. Chem. Soc. A Inorganic, Phys. Theor.* **1968**, 2310−2312.
(22) Mattes, R.; Schröder, F. Die Schwingungsspektren von MoO3, WO2Cl2 Und WO3 Im Festen Zustand: Solid State Vibrational Spectra of MoO3, WO2Cl2 and WO3. *Zeitschrift fur Naturforsch. - Sect. B J. Chem. Sci.* **1969**, *24*, 1095−1100.
(23) Gassman, P. G.; Macomber, D. W.; Willging, S. M. Isolation and Characterization of Reactive Intermediates and Active Catalysts in Homogeneous Catalysis. *J. Am. Chem. Soc.* **1985**, *107*, 2380−2388.
(24) Dickens, P. G.; Whittingham, M. S. The Tungsten Bronzes and Related Compounds. *INORGANIC CHEMISTRY LABORATORY*, OXFORD, 1968.
(25) Orzechowski, L.; Jansen, G.; Harder, S. Methandiide Complexes (R2CM2) of the Heavier Alkali Metals (M = Potassium, Rubidium, Cesium): Reaching the Limit? *Angew. Chem., Int. Ed.* **2009**, *48*, 3825−3829.
(26) Schlosser, M.; Hartmann, J. Transmetalation and Double Metal Exchange: A Convenient Route to Organolithium Compounds of the Benzyl and Allyl Type. *Angew. Chem., Int. Ed. English* **1973**, *12*, 508−509.
(27) Bertz, S. H.; Gibson, C. P.; Dabbagh, G. Preparation and Reactivity of Sodium Organocuprates. *Organometallics* **1988**, *7*, 227−232.